NATIONAL TRANSPORTATION SAFETY BOARD
Office of Research and Engineering
Materials Laboratory Division
Washington, D.C. 20594

February 8, 2021

MATERIALS LABORATORY FACTUAL REPORT Report No. 20-063

A. ACCIDENT INFORMATION

Place	:	Tempe, AZ
Date	:	July 29, 2020
Vehicle	:	Union Pacific Railroad (UP) freight train MTUPX-29
NTSB No.	:	RRD20LR005
Investigator	:	Richard Hipskind (RPH-10)

B. COMPONENTS EXAMINED

2 pieces of rail from the north rail.

C. DETAILS OF THE EXAMINATION

The submitted rail pieces were from the north rail at the derailment site. The pieces were labeled 3W and 4E, with piece numbers increasing from east to west based on the rail reconstruction conducted at the scene.

Piece 3W is shown in Figures 1-4 in the as-received condition. Piece 3W had raised markings on the field side of the web that read “N 2004 2”. The markings indicate the rail was manufactured by Nippon Steel Corporation in February 2004. Manufacturer records indicated the rail size was 136 pound rail[1]. The fracture through piece 3W propagated transversely down from the running surface until approximately mid-web, then turned and propagated longitudinally at roughly 45 degrees along the length of the rail until it reached the bottom of the base. The shape of the fracture surface is shown in Figure 2. Batter and gouges from wheel impact were observed on the running surface of the rail adjacent to the fracture, as shown in the bottom image of Figure 3. Shiny wear was observed on the bottom surface of the base near the cut edge. The yellow dashed line in Figure 4 indicates a wear line across the bottom surface of the base consistent with a tie mark[2].

Piece 4E is shown in Figures 5-8 in the as-received condition, with rail anchors[3] still attached. The fracture through piece 4E propagated transversely straight through most of the cross-section before turning at an angle with respect to the cross-section at

[1] In the rail industry, rail size is referenced in pounds, which is the weight of a 3-foot length of rail.
[2] A tie mark is a straight horizontal line of wear observed on the bottom of a rail piece that results from contact with the mating metal rail tie plate.
[3] Rail anchors are spring steel clips that attach to the bottom of the rail base to prevent longitudinal movement of the rail due to temperature fluctuation or vibration.

the base. A crack (yellow arrows, Figures 5 and 6) was observed branching from the fracture surface at about mid-web. The crack propagated at approximately a 45 degree angle along the longitudinal length of the rail. The running surface adjacent to the fracture surface was smooth with very little damage, as shown in Figure 7. Wear was observed on the bottom surface of the base near the cut edge similar to the wear on piece 3W. Piece 4E also had a wear line across the bottom surface of the base consistent with a tie mark, as indicated by the yellow dashed line in Figure 8.

The features along the profiles of the fractures on each piece were examined and compared. As indicated by the yellow arrows in Figure 9, many features along the profiles at the web and in the adjacent neck area aligned. In addition, macro features on the fracture surfaces also fit together. These observations are consistent with the fracture surfaces on pieces 3W and 4E mating. Consequently, the only portion of rail that was missing and not submitted was the bottom of piece 3W, which consisted of the neck from where the fracture began to propagate longitudinally at 45 degrees and the base. Images of the two pieces as they mate together are shown in Figures 10-12.

The length of each piece was measured from the transverse cut surface to the fracture surface along the base on the field and gage sides. The length of piece 3W was also measured from the cut surface to the edge of the fracture surface at approximately mid-web where the fracture changed direction from transverse to longitudinal at a roughly 45 degree angle through the rail. Additionally, the distance between the tie marks on the bottom surfaces of the rail bases with the fracture surfaces of pieces 3W and 4E mating was also measured for comparison to the track build records. The measurements are shown in Figures 10-12.

1. Optical Fractography

The fracture surface was transversely sectioned from piece 3W for examination as shown in Figure 13. Several adjacent parallel transverse cross-sections were also prepared for further metallurgical work and labeled as slices A, B, and C, as shown. A dark colored anomaly (encircled in a yellow dotted line) was observed on the fracture surface near the mid-web. A digital microscope image of the anomaly is shown in Figure 14. The anomaly had raised edges compared to the surrounding fracture surface, which had been flattened. Measurements locating the anomaly with respect to the running surface and the field side of the web are shown in Figure 15.

The remainder of the fracture surface on piece 3W had features consistent with overstress. Chevron marks[4] were observed in the web on the fracture surface, as outlined in white in Figure 13. The directionality of the chevrons indicated the fracture origin was in the rail head. Fan shaped features in the rail head on the fracture surface, delineated by yellow arrows, indicated the fracture originated from near the gage side corner adjacent to the running surface.

[4] Chevron marks occur in brittle fractures, with tips that point towards the origin of the fracture.

A portion of the upper and gage sides of the rail head on piece 3W were deformed and curled over the fracture surface consistent with trailing rail end deformation.[5] The origin area of the overstress fracture was mostly obscured the trailing rail end deformation on the fracture surface on this piece. The depth of the trailing rail end deformation was determined using a straight edge held flush along the running surface and measuring transversely along the fracture surface. The depth of the trailing rail end deformation measured approximately 0.07 inches, as shown in the digital microscope image in the top of Figure 16.

The rail anchors were removed from piece 4E and the fracture surface was transversely sectioned for examination as shown in Figure 17. After sectioning, the head portion of the piece separated from the base due to the 45 degree longitudinal crack branching from the transverse fracture surface (yellow arrows).

The base portion of piece 4E is shown in Figure 18. Chevron marks (white lines) were observed on both the longitudinal and transverse fracture surfaces. The chevrons on the longitudinal web fracture surface pointed back towards the transverse web fracture, thus indicating the longitudinal web fracture was secondary and started by branching off the transverse web fracture. The chevrons on the transverse web facture surface pointed in the direction of the rail head.

The head portion of piece 4E is shown in Figure 19. Chevron marks (white lines) were visible on the transverse web fracture surface that pointed in the direction of the rail head. Macro features (yellow arrows) on the fracture surface in a fan pattern indicated the fracture originated from near the gage side corner adjacent to the running surface. Digital microscope images of the gage side corner are shown in Figure 20. The macro fan features (black arrows) point towards a fracture origin location adjacent to the running surface at the top edge of the transition to the gage side corner. This location is encircled in a black dashed line in the top of Figure 20. A small area of receiving rail end batter[6] (red arrows) was observed on the gage side corner near the fracture origin.

2. Electron Microscopy and EDS

The fracture surfaces from both pieces were examined using a scanning electron microscope (SEM). Piece 4E is shown in Figures 21-22. Red arrows in Figure 21 point to receiving rail end batter on the gage side corner near the fracture origin. The fracture surface features immediately adjacent to the batter exhibited cleavage facets, consistent with overstress fracture of a less ductile metal alloy. Examination of the fracture surface in the web of the rail, away from the fracture origin in the head, revealed the similar cleavage facets and overstress features, as shown in Figure 22.

[5] Trailing rail end deformation is deformation at the vertical face of the delivering rail end. It can occur when a misalignment or gap between the two rails allows the wheel to drop below the surface of the delivering rail.
[6] Receiving rail end batter is an impact deformation on the vertical face of a receiving rail end. It can occur when a misalignment or gap between two rails allows the wheel to drop below the surface of the delivering rail, and hammer against the end of the receiving rail as it rolls over the end corner of the rail.

The fracture surface in the head and the web of piece 3W is shown in Figures 23 and 24, respectively. Heavy oxidation obscured the finer features on this piece, but the overall features consisted of cleavage features like those observed on piece 4E. Backscattered electron (BSE) examination of the fracture surface revealed heavy oxidation all over. BSE images of the dark colored anomaly in the web also only showed oxidation products.

Energy dispersive x-ray spectroscopy (EDS) was performed on the piece 3W fracture surface. In the head of the piece the EDS spectrum was consistent with a carbon steel (top image of Figure 25). EDS was also performed of the dark colored anomaly, as shown in the bottom image of Figure 25. A very large carbon peak and a large oxygen peak were observed in this location, which is expected given the oxidation observed on the fracture surface in this area (shown in Figure 24). Distinct peaks for silicon, aluminum, magnesium, and sulfur were also present in the spectrum, along with traces of sodium, potassium, and calcium. This combination of elements is consistent with exogenous contamination, such as soil.

3. Metallography and Hardness

Transverse rail cross-section slice A from piece 3W was cut below the head to remove the head portion from the rest of the piece. The head portion was polished and etched with Nital, and the result is shown in Figures 26-29. The microstructure observed on the polished and etched cross-section was pearlite, consistent with standard rail steel. No cracks consistent with head checking[7] were observed at the gage corners (Figures 27 and 28) and no elongated or smeared grains consistent with surface rolling contact deformation were observed at either the gage corners (Figure 28) or the running surface (Figure 29).

A transverse cross-section was also prepared at the dark colored anomaly on the fracture surface in the web of piece 3W, as shown in Figure 30. The microstructure in this location was examined by polishing into the anomaly in the direction indicated by the yellow arrow. The microstructure within and away from the fracture surface anomaly in the same plane of polish is shown in Figures 31 and 32, respectively. No differences were noted in the microstructures in the two areas, and both also appeared the same as the microstructure of the head.

The rail head cross-section from piece 3W was Rockwell hardness tested per ASTM E18.[8] The hardness indents were performed at locations prescribed in AREA *Manual for Railway Engineering*.[9] This standard prescribes three measurements approximately at mid-head height, and two additional measurements 0.375 inches each

[7] Head checks are a rail surface condition where horizontal cracks form in the deformation zone near the surface of the rail head. Where the cracks intersect the surface, they may form a saw-tooth or check-shaped pattern.
[8] ASTM E18 – *Standard Test Methods for Rockwell Hardness and Rockwell Superficial Hardness of Metallic Materials*. ASTM International, West Conshohocken, PA.
[9] Manual of Railway Engineering, Chapter 4, Rail, American Railway Engineering and Maintenance-of-Way Association, Lanham, Maryland (1997).

from the field and gage faces of the cross section. A diagram showing the locations for the seven prescribed hardness indents is illustrated in the top of Figure 33.

The results of the hardness testing on the piece 3W rail head are illustrated in the bottom of Figure 33. The average hardness value of the material was 40 HRC. According to the 1997 AREMA specifications, the minimum specified tensile strength for standard rail steel was 140,000 pounds per square inch, which corresponds to an approximate hardness of 31 HRC.

4. Rail Cross-Section Measurement

An overall photo of the as-cut surface of transverse rail cross-section slice B from piece 3W is shown in Figure 34. For reference, an outline (yellow dashed line) representing the cross-section of a new 136-pound rail is overlaid atop the as-cut transverse cross-section. No measurable head loss was observed on the cross-section.

Adrienne V. Lamm
Materials Engineer

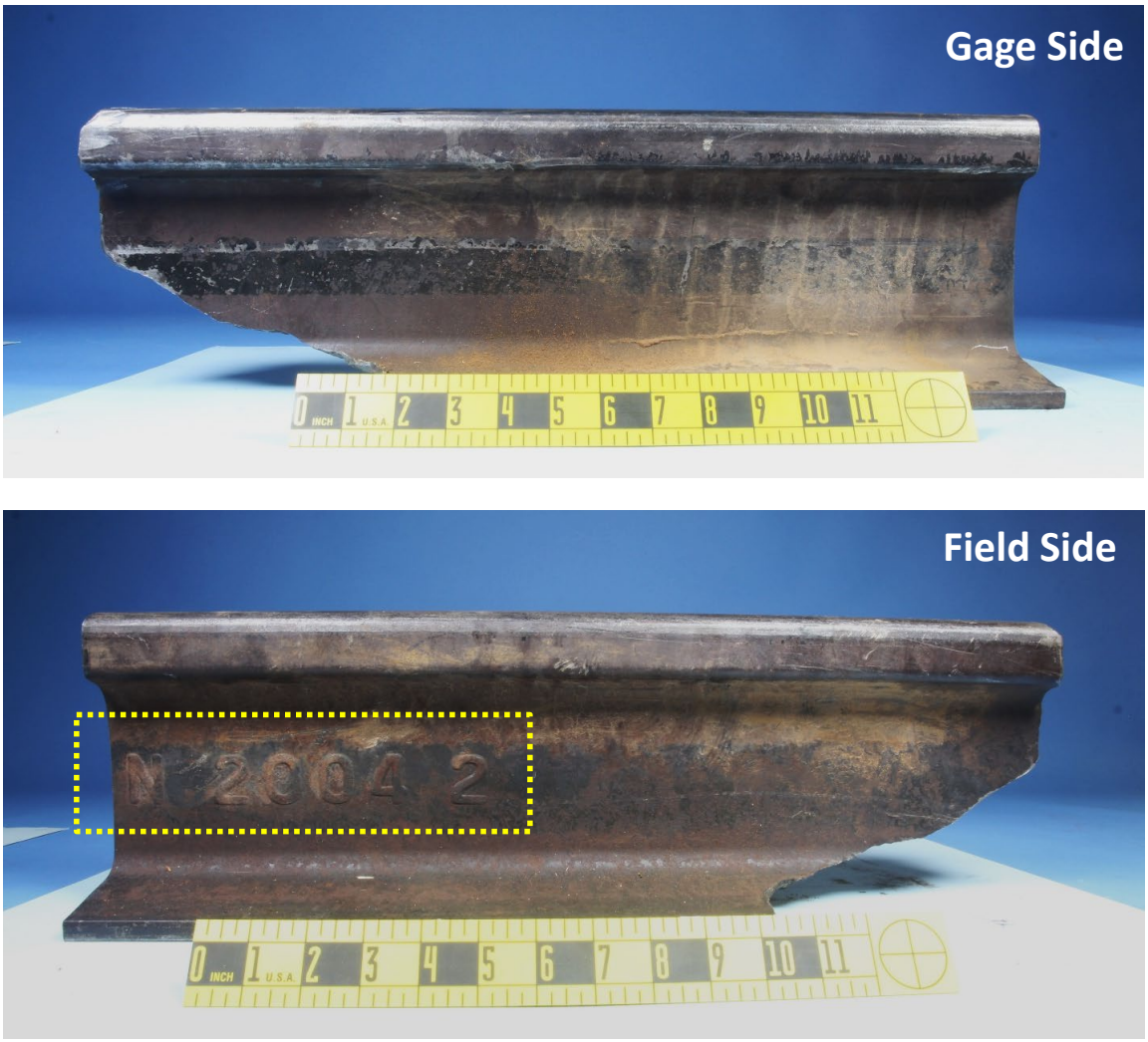

Figure 1: Macro photos of the gage and field sides (top and bottom, respectively) of piece 3W. The yellow dotted line outlines raised markings on the field side web.

Figure 2: Macro photos of the fracture surface on piece 3W.

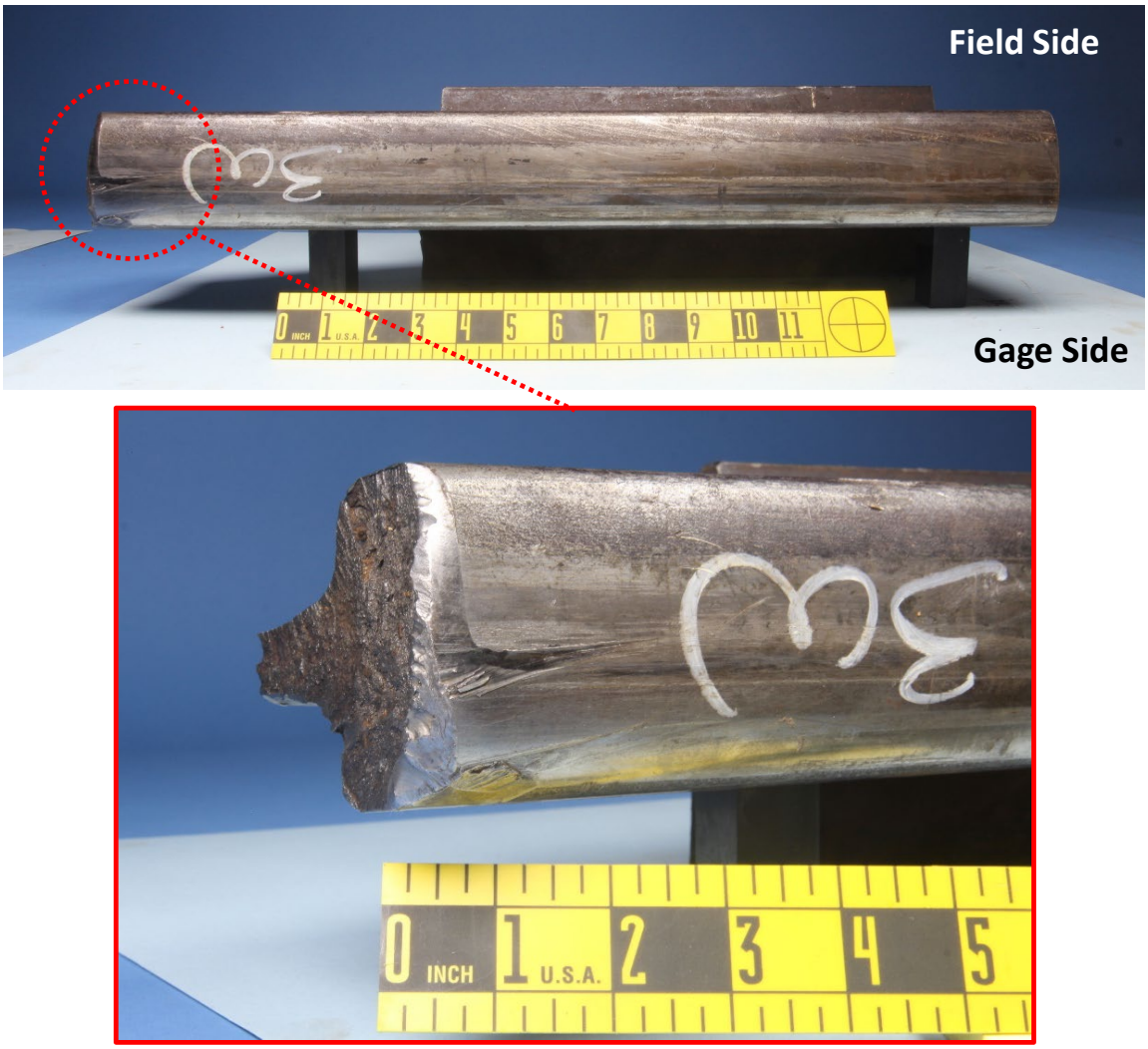

Figure 3: Macro (top) and close-up (bottom) photos of the running surface on piece 3W.

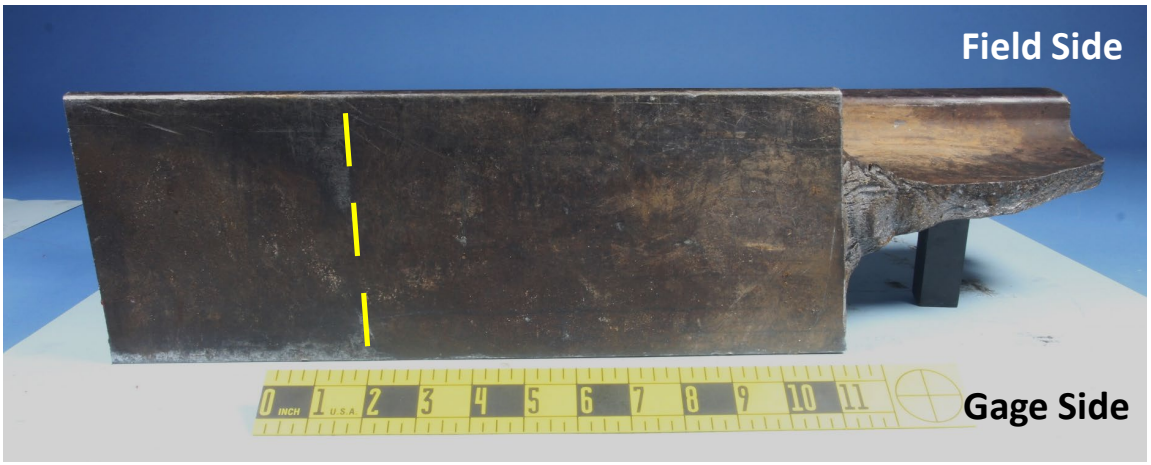

Figure 4: Macro photo of the bottom surface of the base of piece 3W. The yellow dashed line indicates a tie mark.

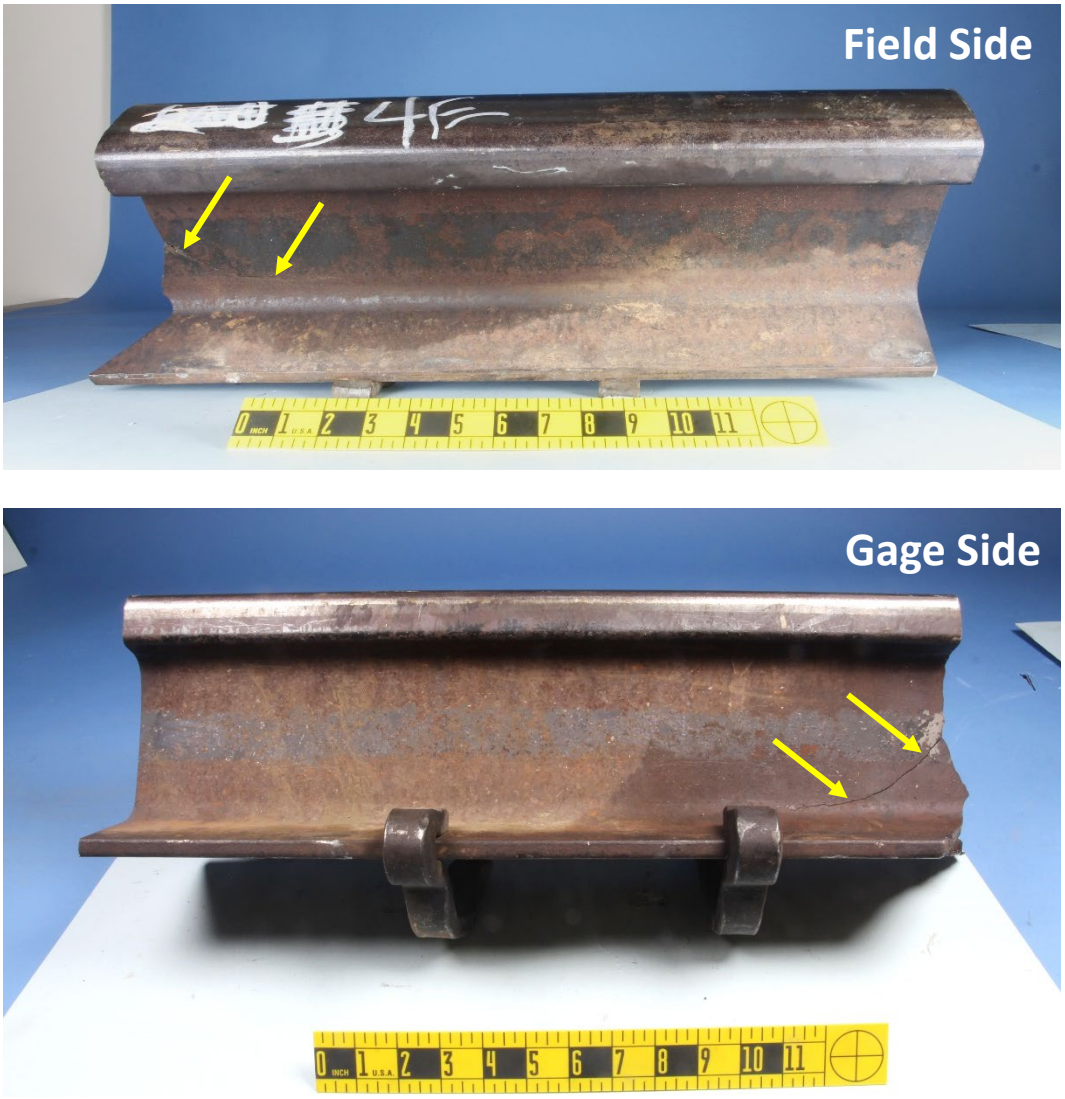

Figure 5: Macro photos of the field and gage sides (top and bottom, respectively) of piece 4E. The yellow arrows point to a longitudinal crack branching from the transverse fracture surface.

Figure 6: Macro photos of the fracture surface on piece 4E. The yellow arrows point to a longitudinal crack branching from the transverse fracture surface.

Figure 7: Macro (top) and close-up (bottom) photos of the running surface on piece 4E.

Figure 8: Macro photo of the bottom surface of the base of piece 4E. The yellow dashed line indicates a tie mark.

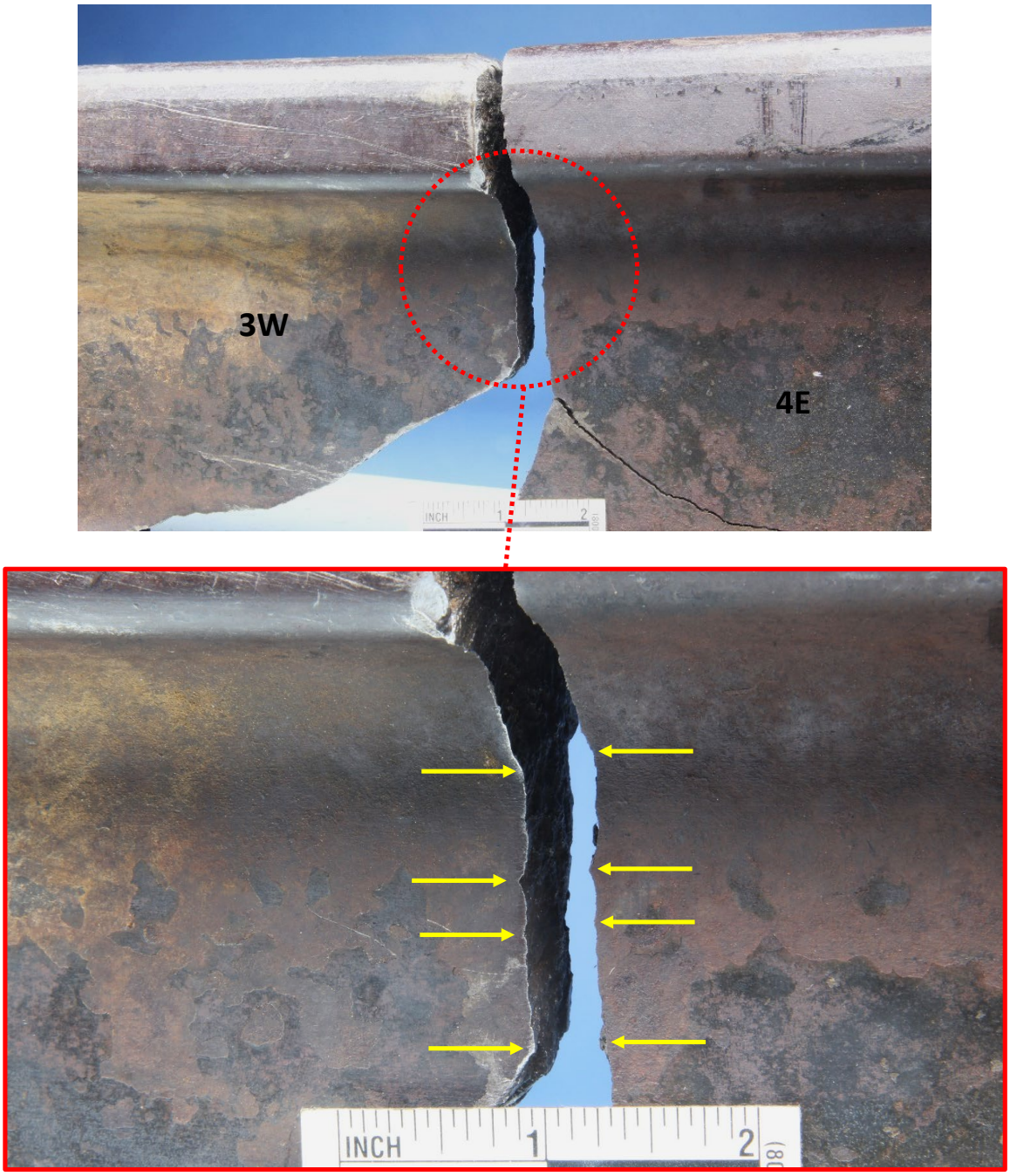

Figure 9: Close-up photos of the field side web surface of pieces 3W and 4E. The yellow arrows point to aligned features along the fracture surface profiles.

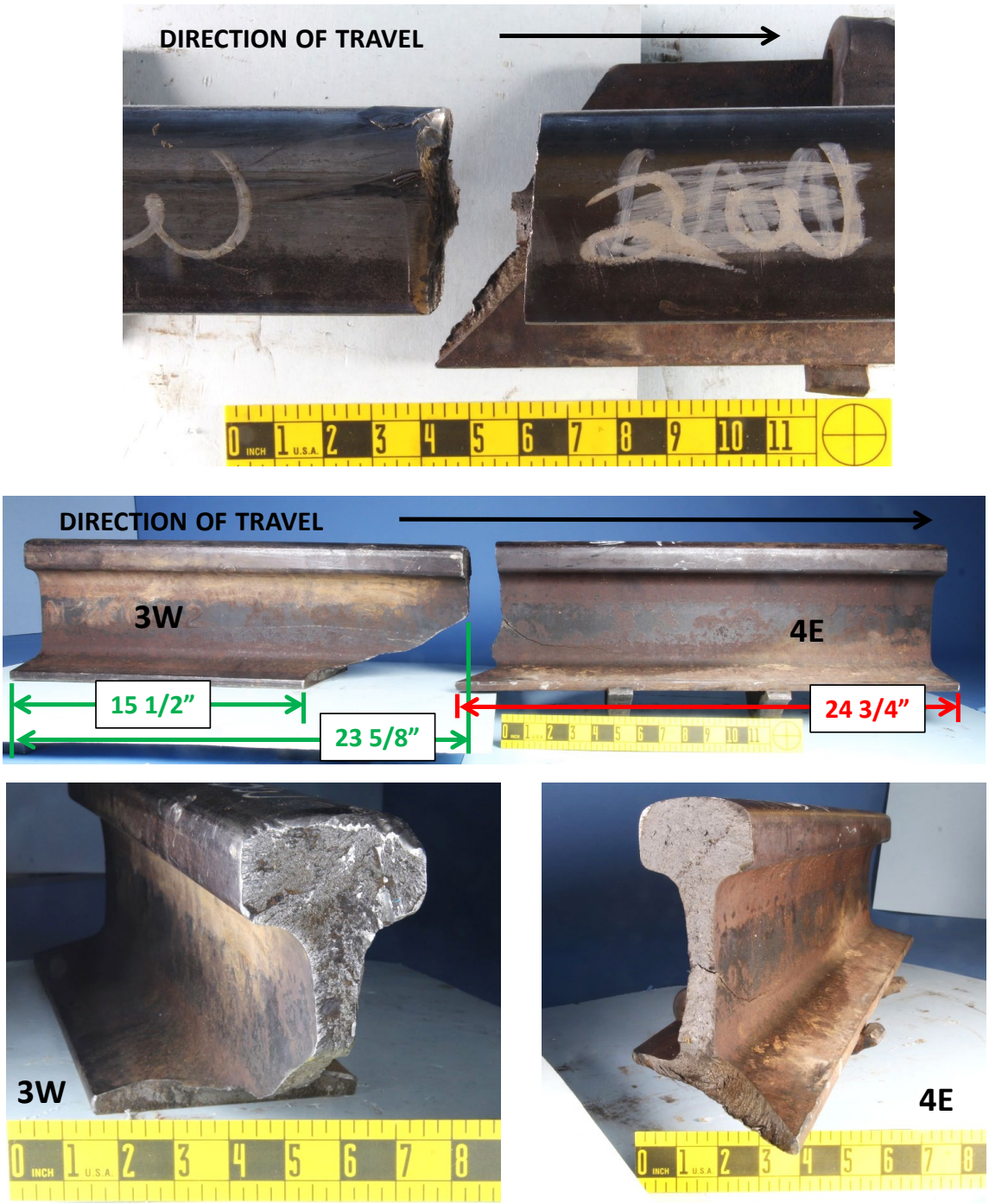

Figure 10: Macro and close-up photos showing how pieces 3W and 4E mated as viewed from the field side. Various measurements of the pieces are listed.

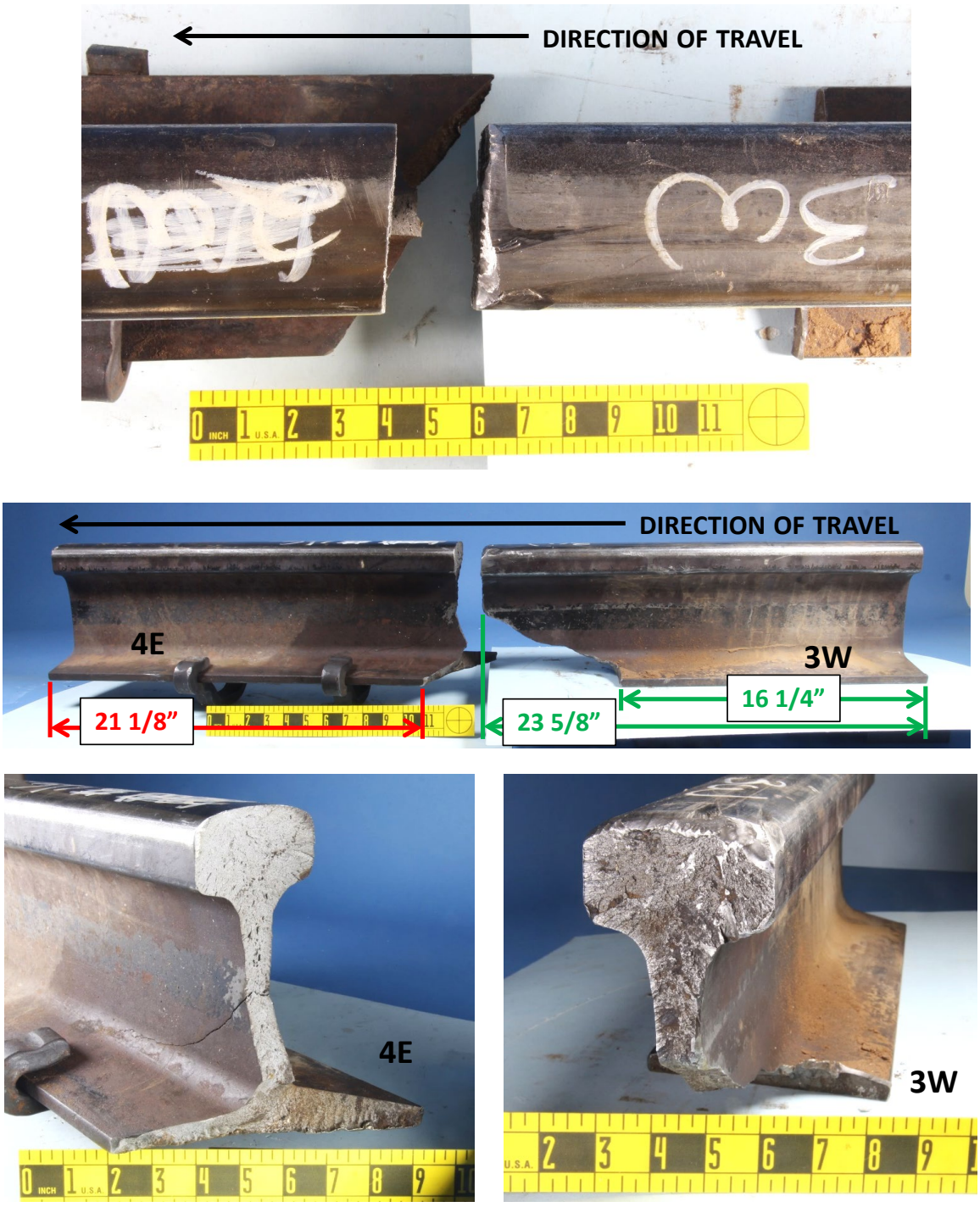

Figure 11: Macro and close-up photos showing how pieces 3W and 4E mated as viewed from the field side. Various measurements of the pieces are listed.

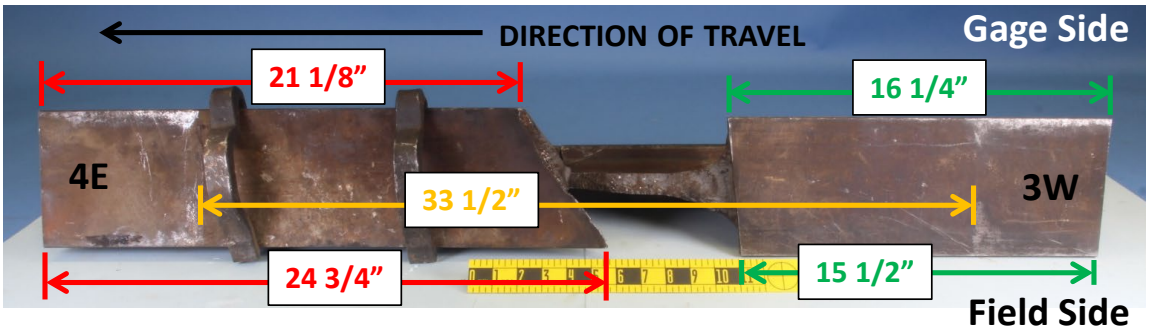

Figure 12: Macro photos showing how pieces 3W and 4E mated as viewed from the bottom. Various measurements of the pieces and the distance between the tie marks on the bottom surfaces of the pieces are listed.

Figure 13: (Top) Macro photo of piece 3W after transversely sectioning the fracture surface and adjacent parallel transverse cross-sections labeled slices A, B, and C, as shown.

(Bottom) Close-up photos of the piece 3W fracture surface. White lines outline chevron marks and the yellow dotted line outlines a dark colored anomaly on the web surface. The yellow arrows follow macro features in a fan pattern on the head surface.

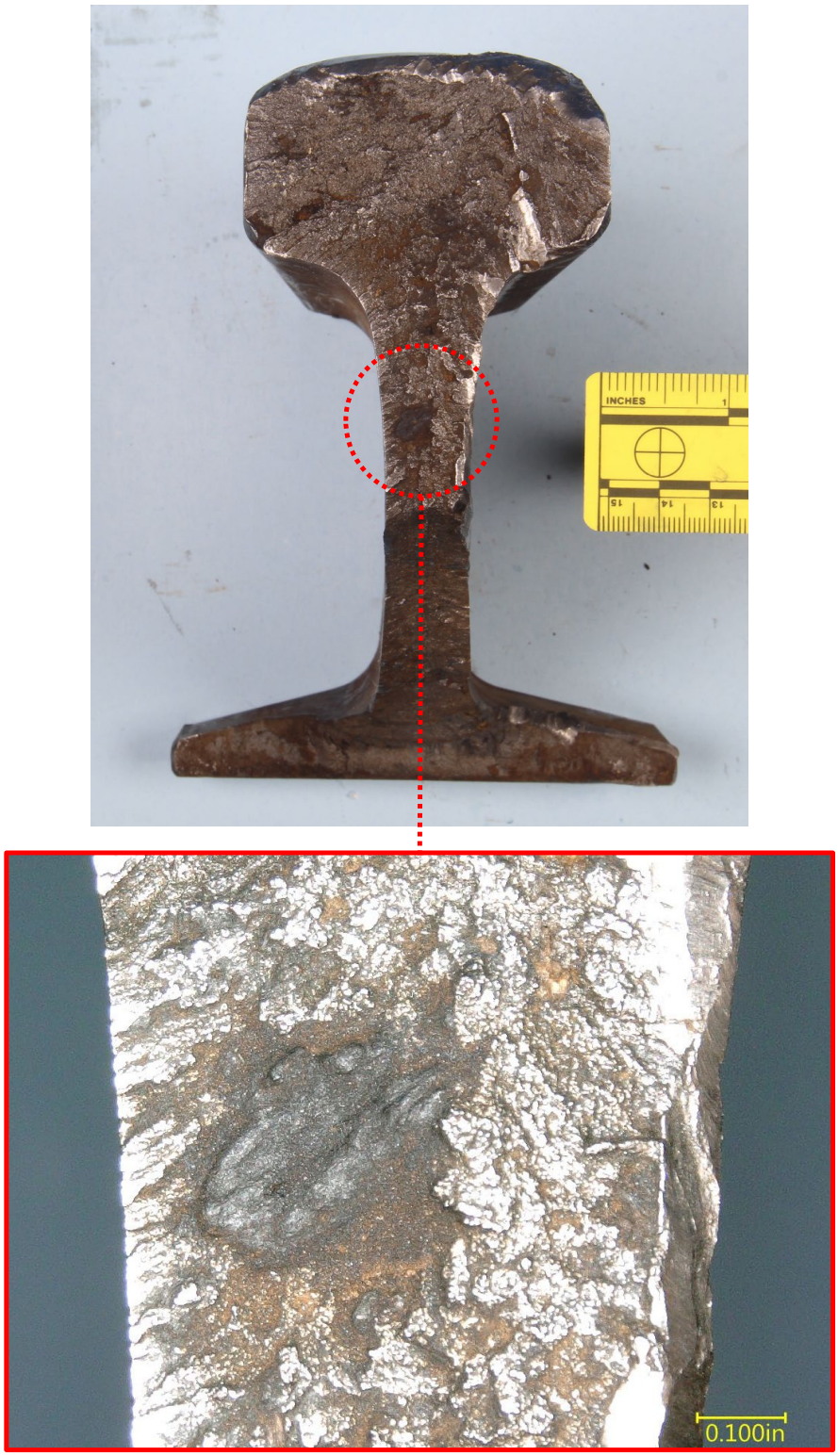

Figure 14: Close-up photo (top) and digital microscope image (bottom) of the dark colored anomaly on the web fracture surface of piece 3W.

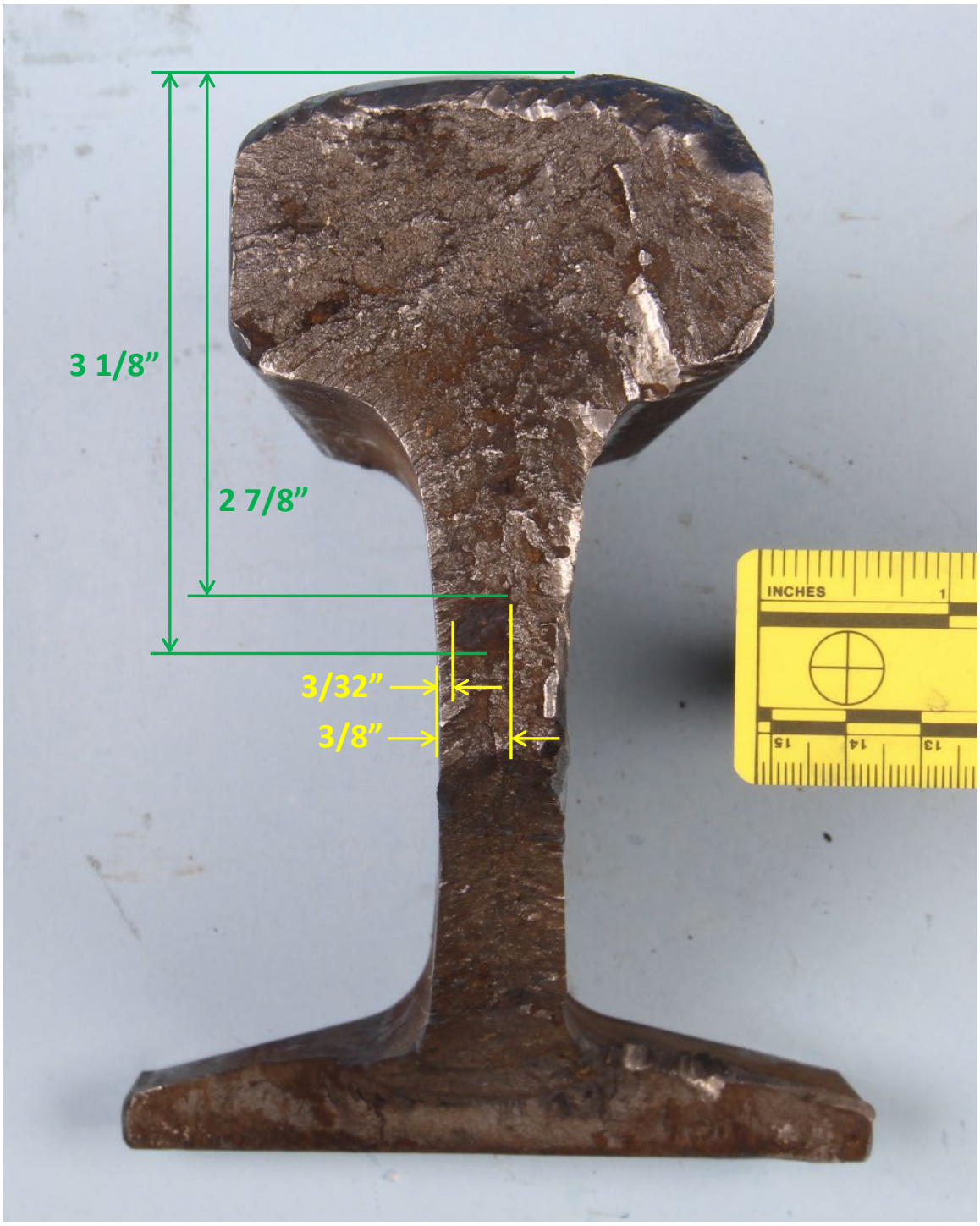

Figure 15: Close-up photo of the web fracture surface of piece 3W with measurements indicating the location of the dark colored anomaly.

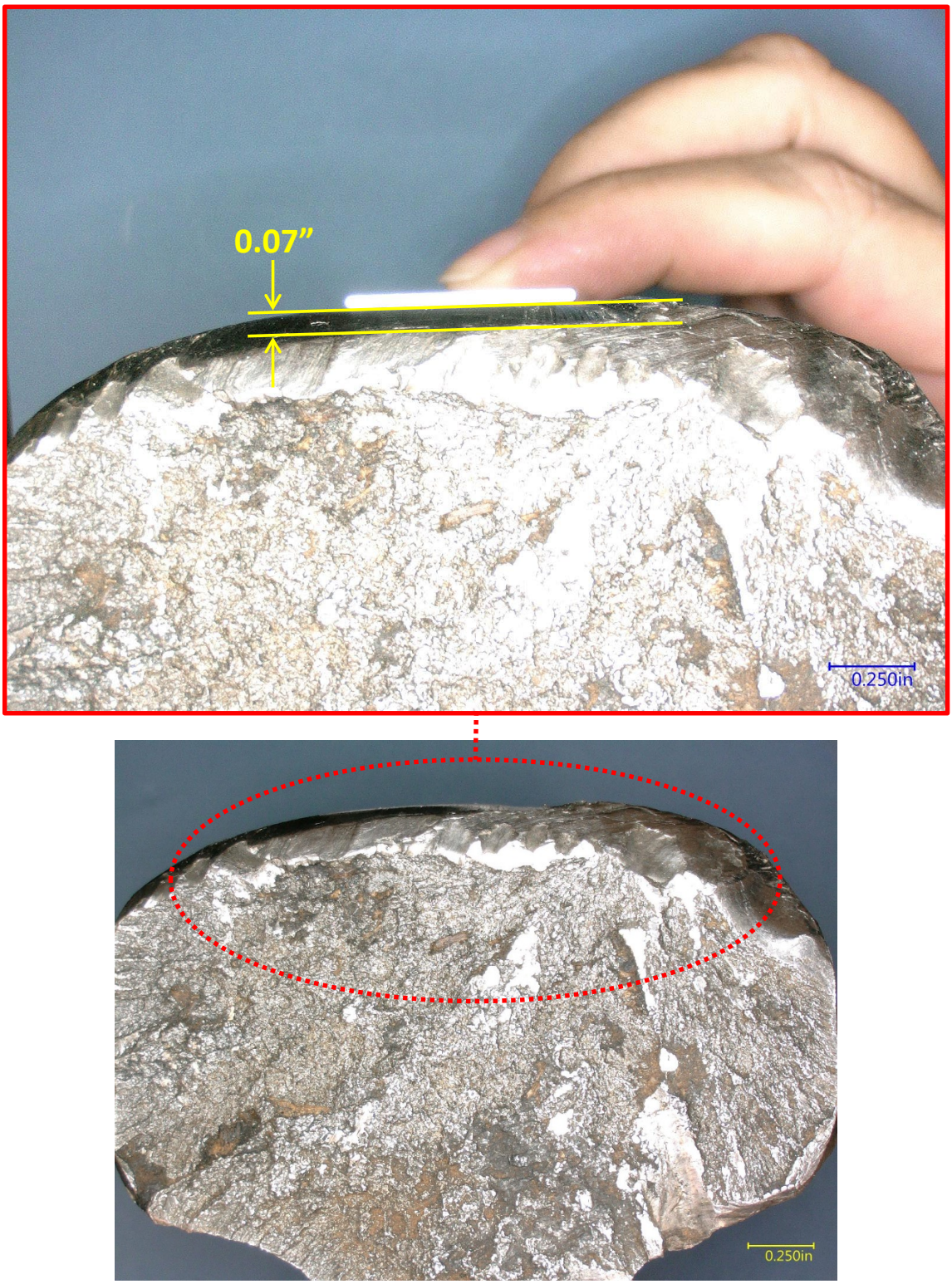

Figure 16: Digital microscope images of trailing rail end deformation on the upper and gage sides of the rail head on piece 3W. A measurement of the depth of the trailing rail end deformation is shown.

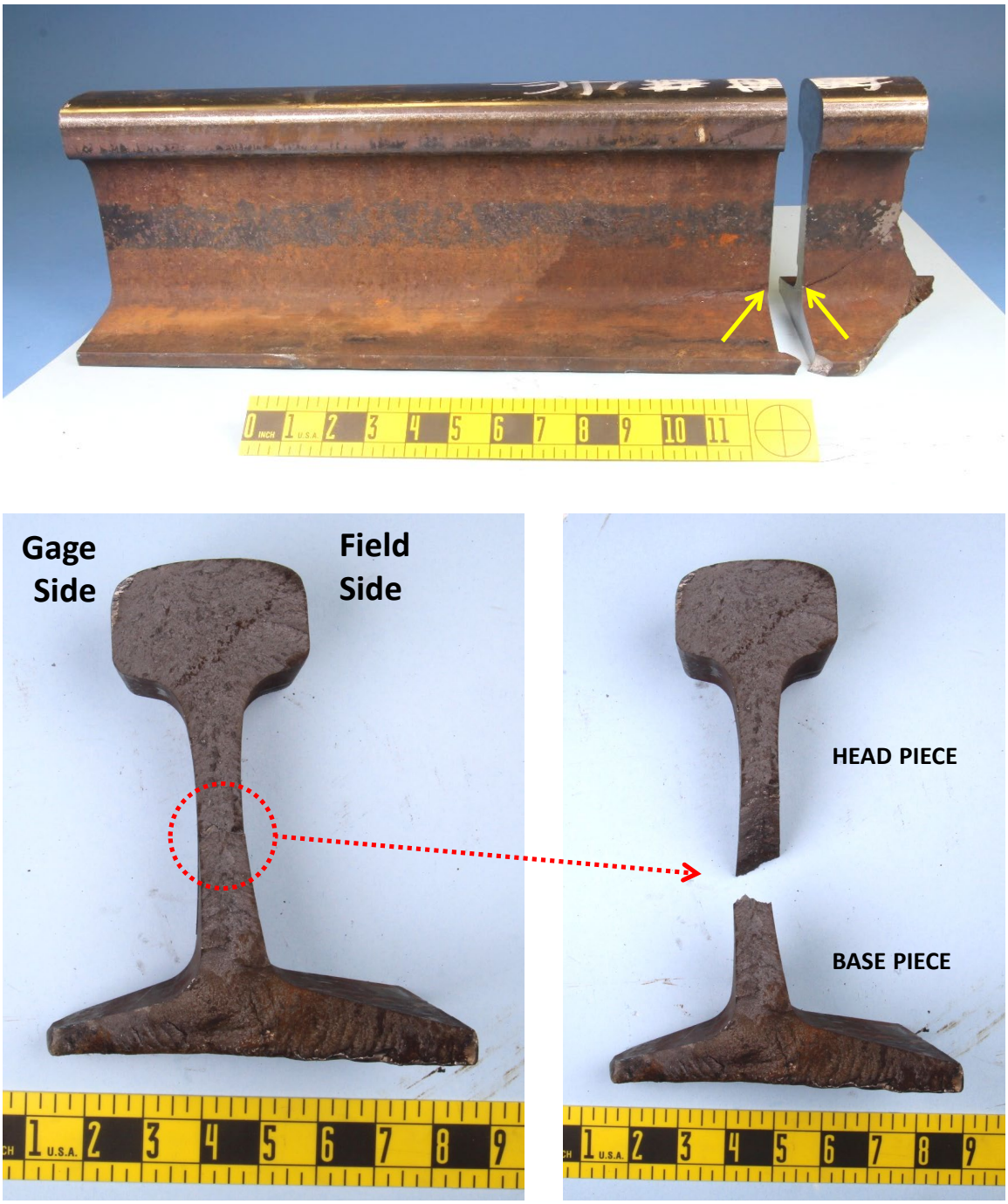

Figure 17: Macro photos of piece 4E after transversely sectioning the fracture surface. After sectioning, the head portion of the piece separated from the base due to the 45 degree longitudinal crack branching from the transverse fracture surface (yellow arrows).

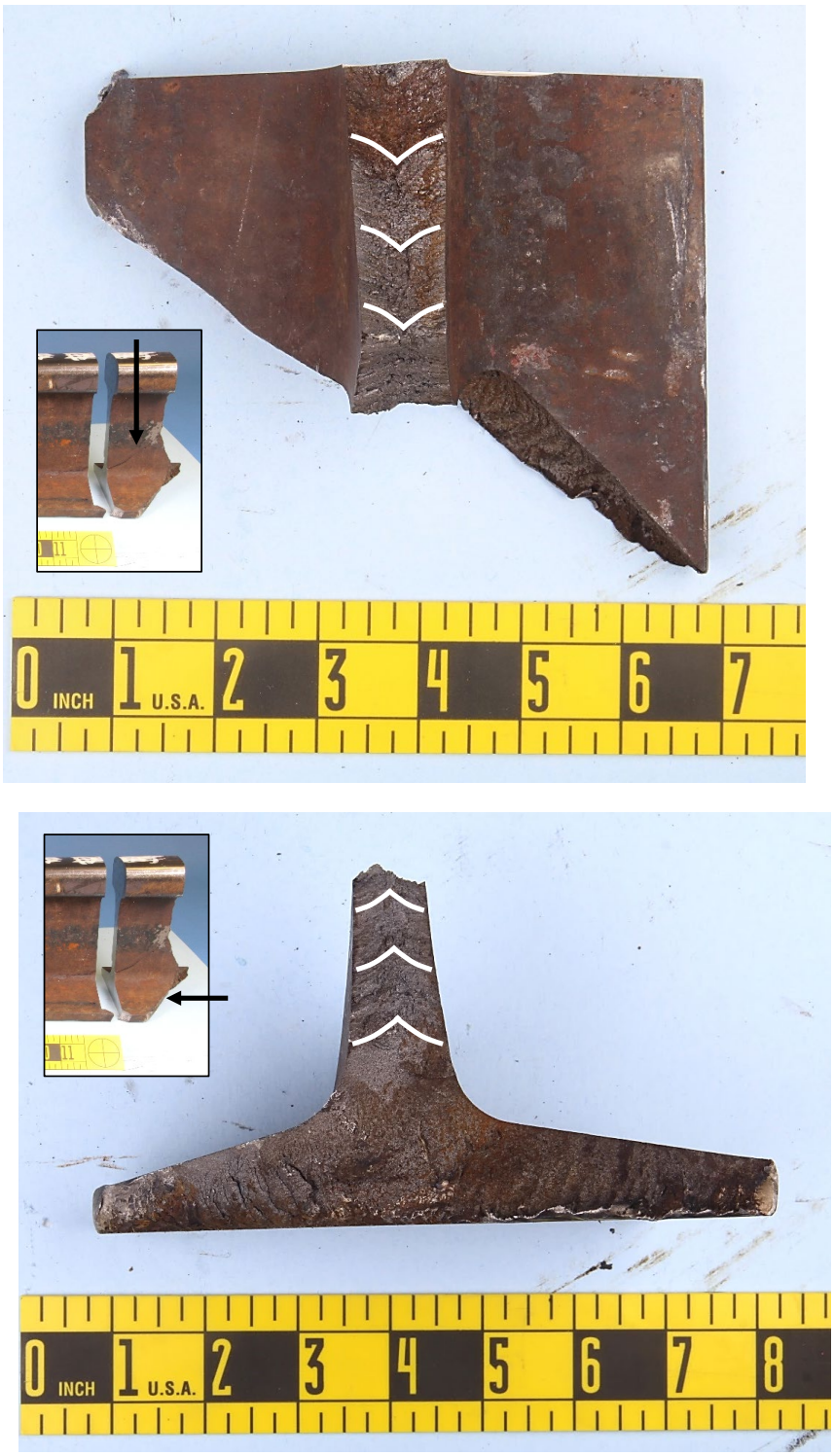

Figure 18: Close-up photos of the fracture surfaces on the base portion of piece 4E. Chevron marks on the longitudinal web fracture (white lines, top image) pointed back towards the transverse web fracture surface, while chevrons marks on the transverse web facture surface (white line, bottom image) pointed in the direction of the rail head. The inset photos show the direction of the view in each close-up photo, indicated by the black arrows.

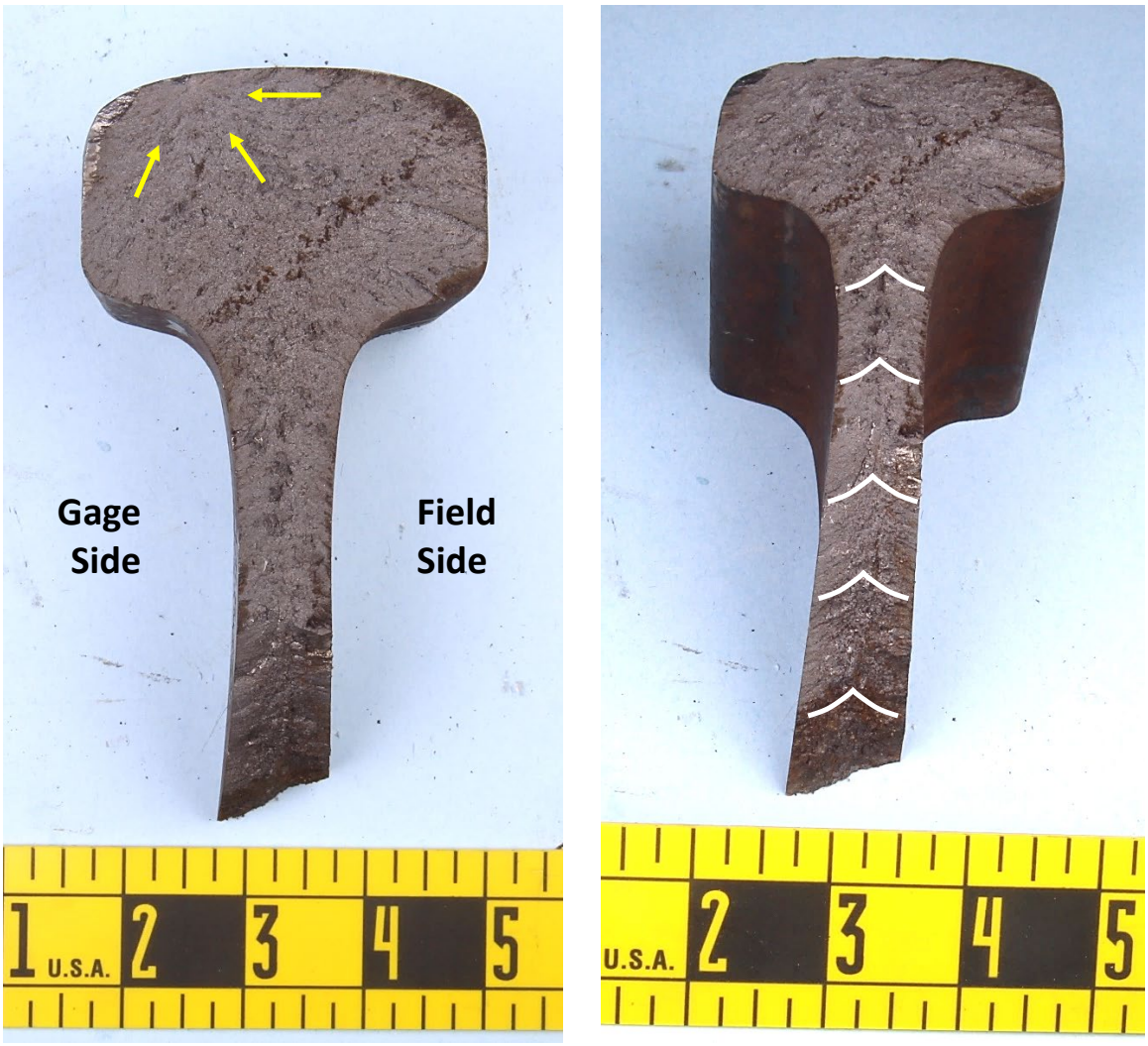

Figure 19: Close-up photos of the fracture surface on the head portion of piece 4E. White lines outline chevron marks on the web surface. The yellow arrows follow macro features in a fan pattern on the head surface.

Figure 20: Digital microscope images of the fracture surface on the head portion of piece 4E. The black arrows follow macro features in a fan pattern that point to a fracture origin location (black dashed circle) adjacent to the running surface at the top edge of the transition to the gage side corner.

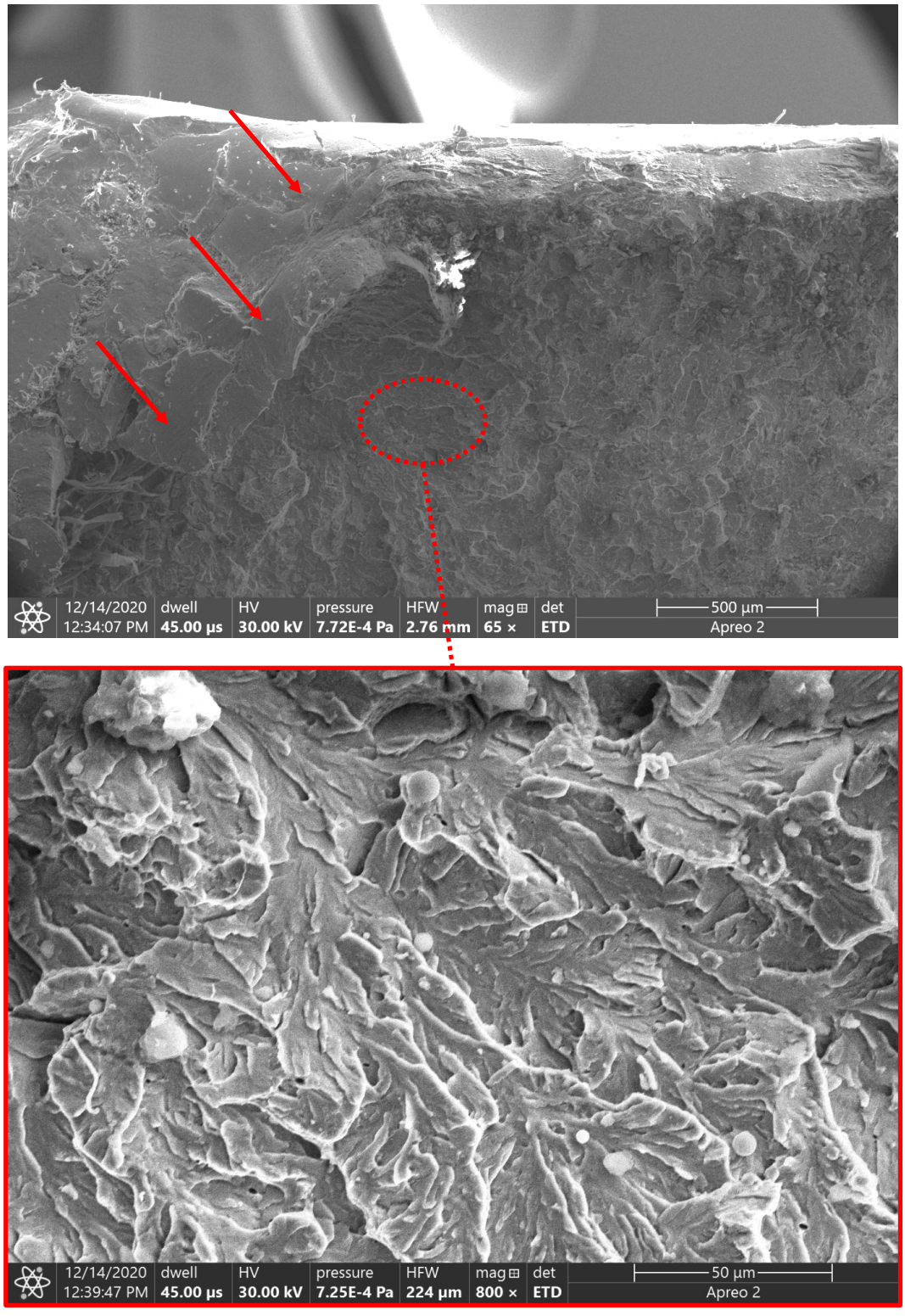

Figure 21: Secondary electron (SE) SEM images of the fracture surface at the gage side corner on piece 4E. The red arrows point to receiving rail end batter.

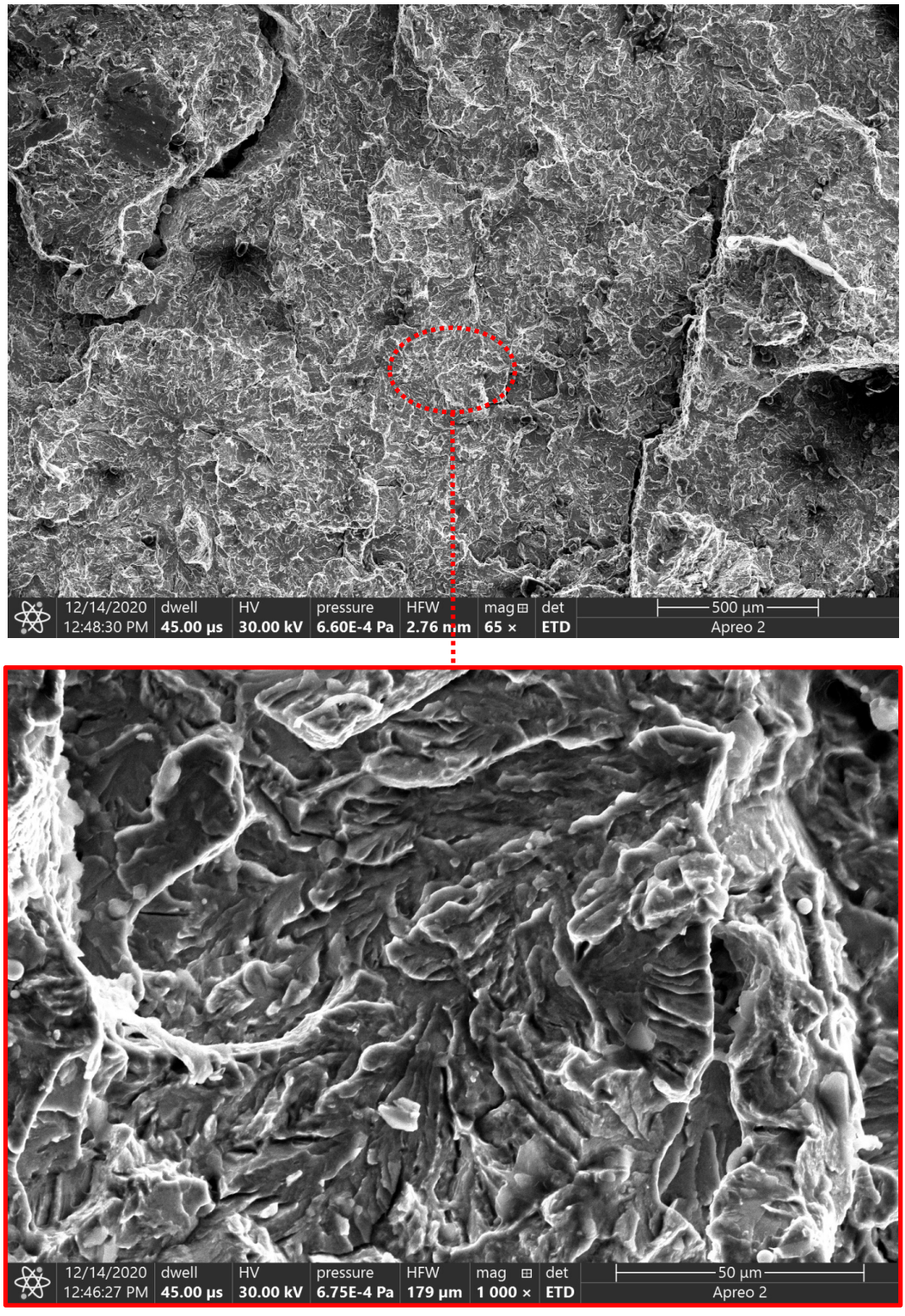

Figure 22: SE SEM images of the fracture surface in the web on piece 4E.

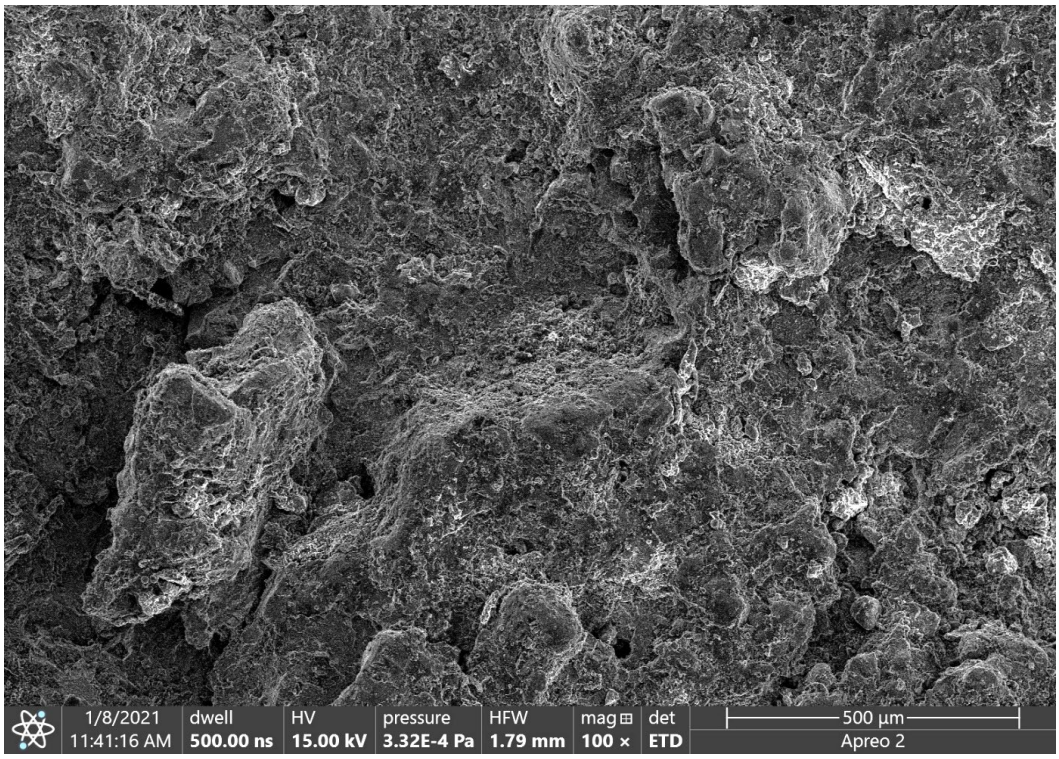

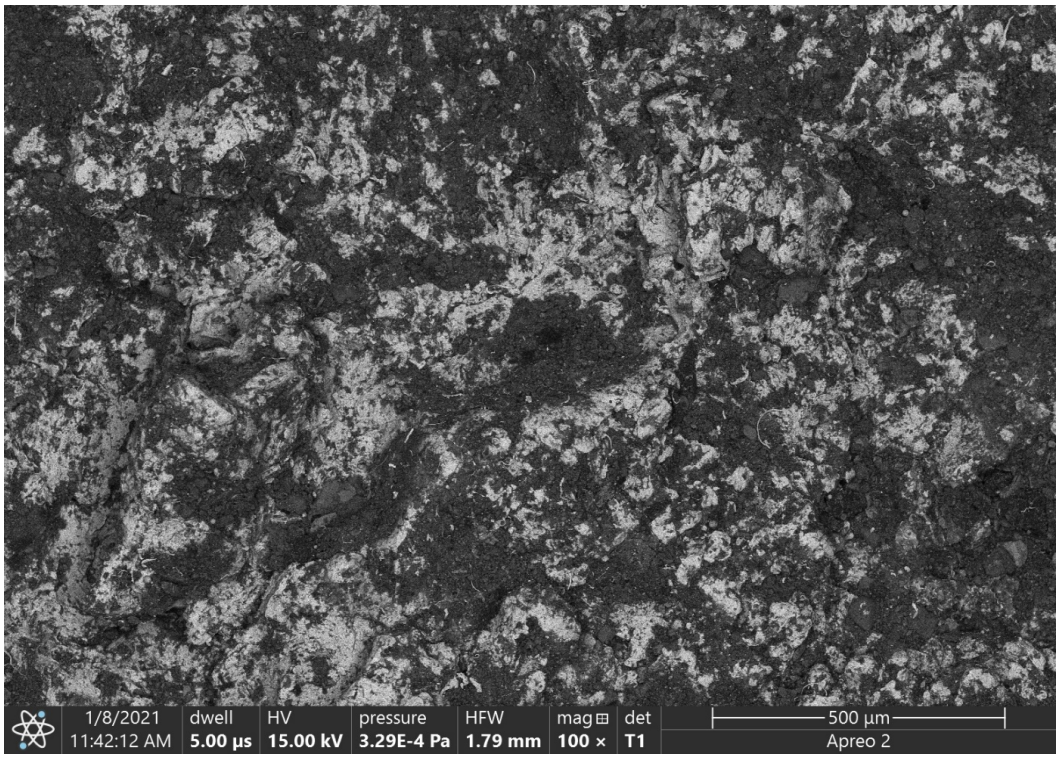

Figure 23: SE (top) and BSE (bottom) SEM images of the fracture surface in the head of piece 3W.

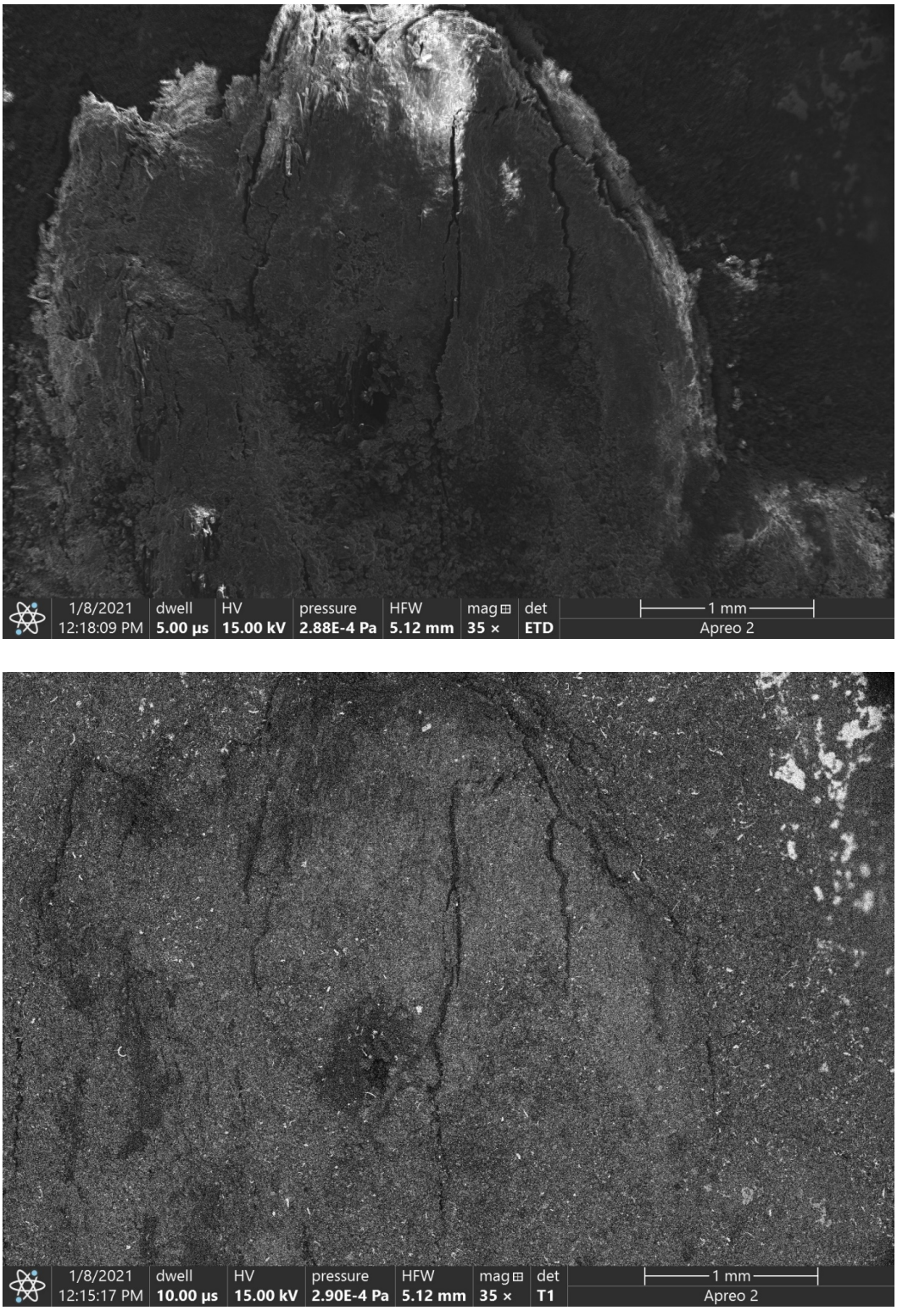

Figure 24: SE (top) and BSE (bottom) SEM images of the fracture surface at the edge of the dark colored anomaly in the web of piece 3W.

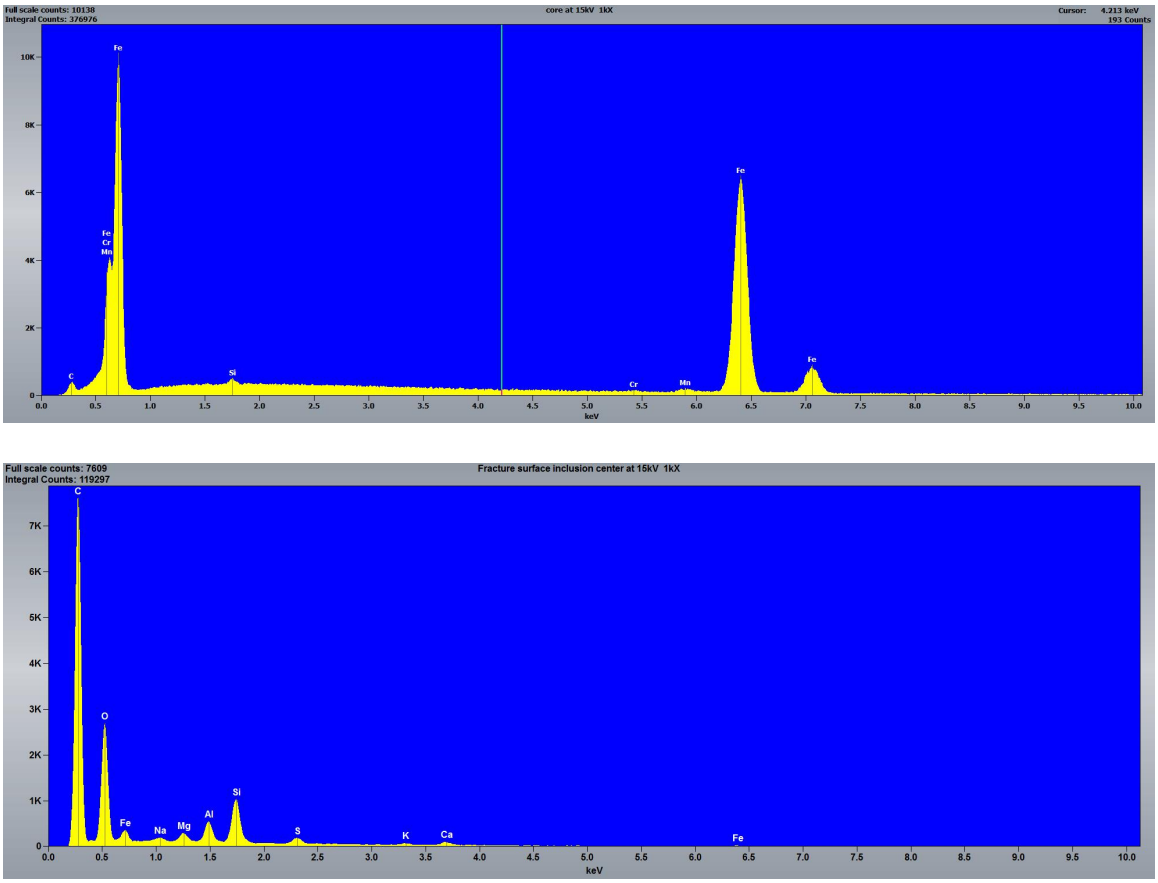

Figure 25: EDS spectra in the head and the dark colored anomaly in the web of piece 3W are shown in the top and bottom images, respectively.

Figure 26: Bright field metallographic image of the base metal of piece 3W. (Etch: 2% Nital)

Figure 27: Bright field metallographic images of gage corner of piece 3W in two locations. (Etch: 2% Nital)

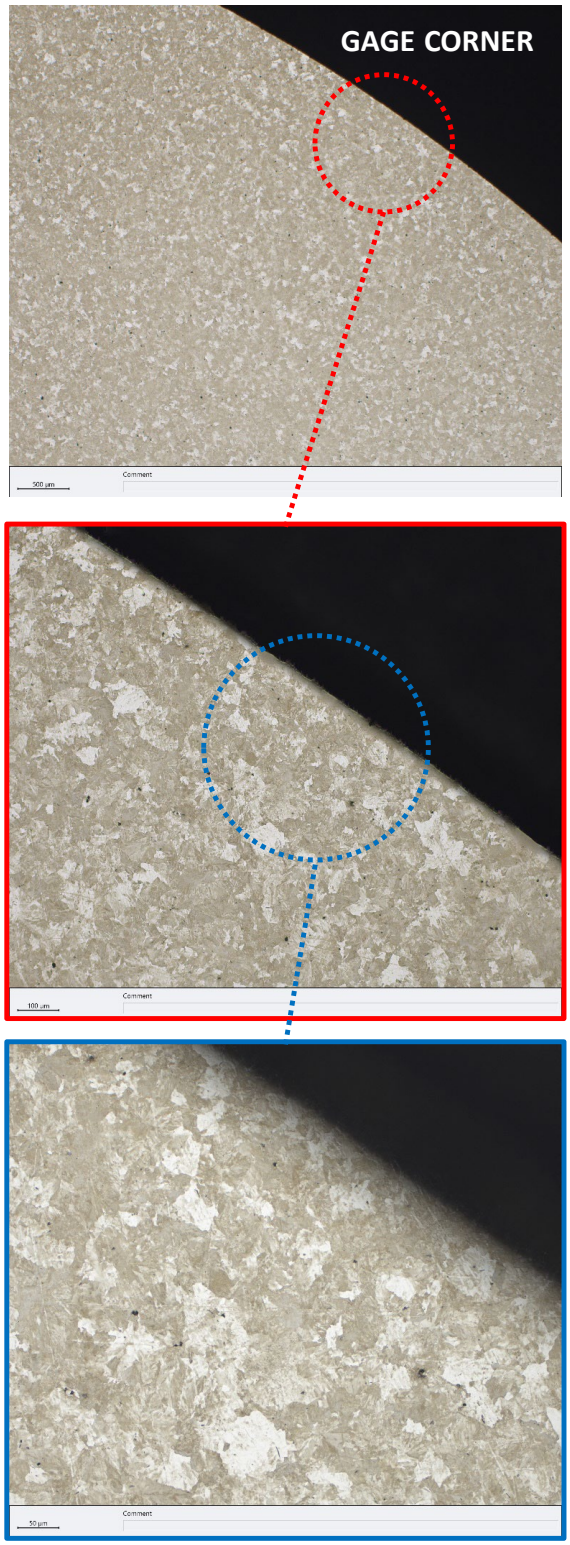

Figure 28: Bright field metallographic images showing successively higher magnifications of gage corner of piece 3W in one location.
(Etch: 2% Nital)

Figure 29: Bright field metallographic image of the running surface of piece 3W. (Etch: 2% Nital)

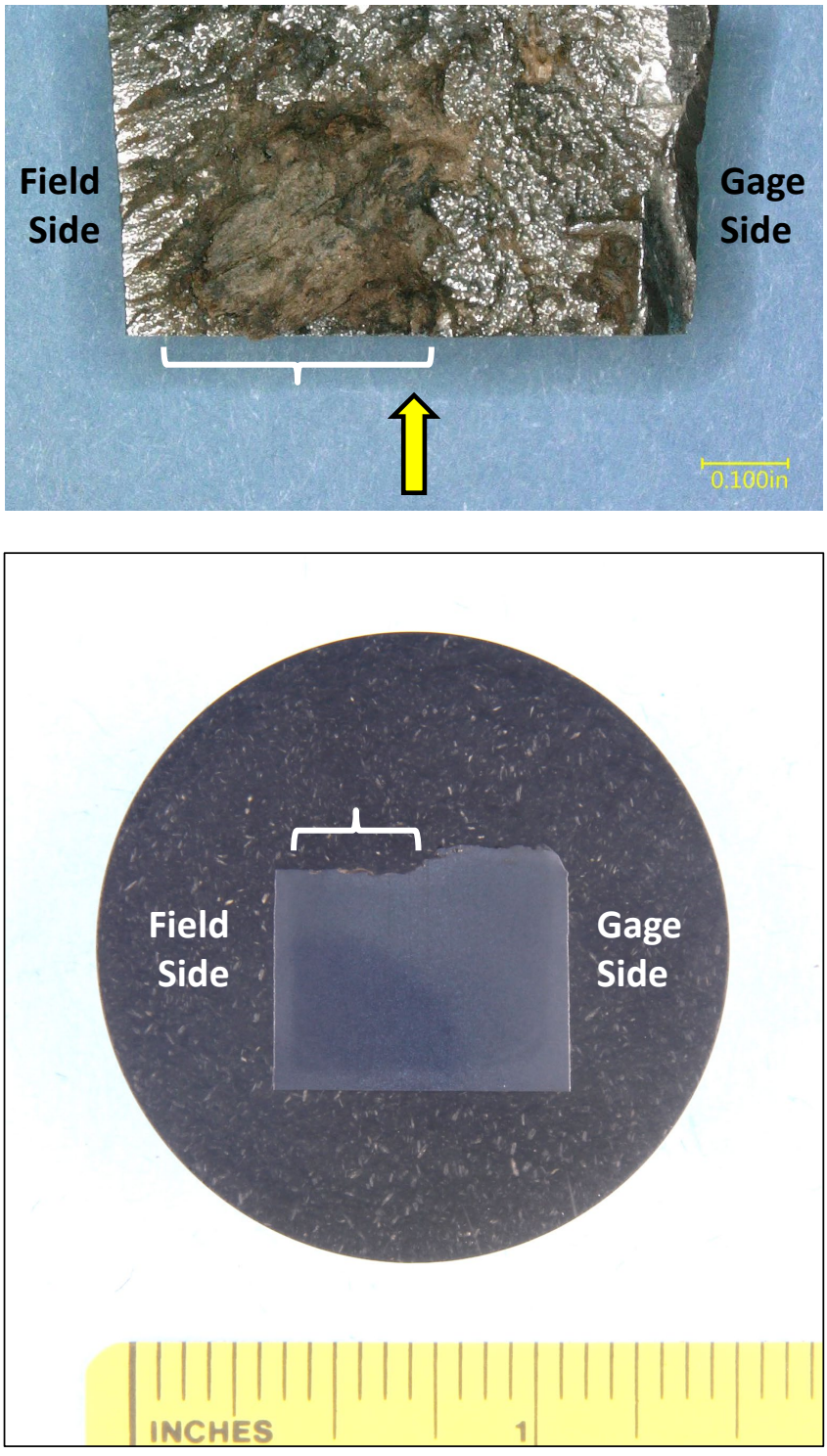

Figure 30: (Top) Digital microscope image of the transverse cross-section through the web of piece 3W. (Bottom) Macro photo of the cross-sectioned, polished, and etched sample of piece 3W in a metallographic mount (Etch: 2% Nital). The white brackets indicate the anomaly on the fracture surface. The yellow arrow in the top image indicates the polishing direction for the mount in the bottom image.

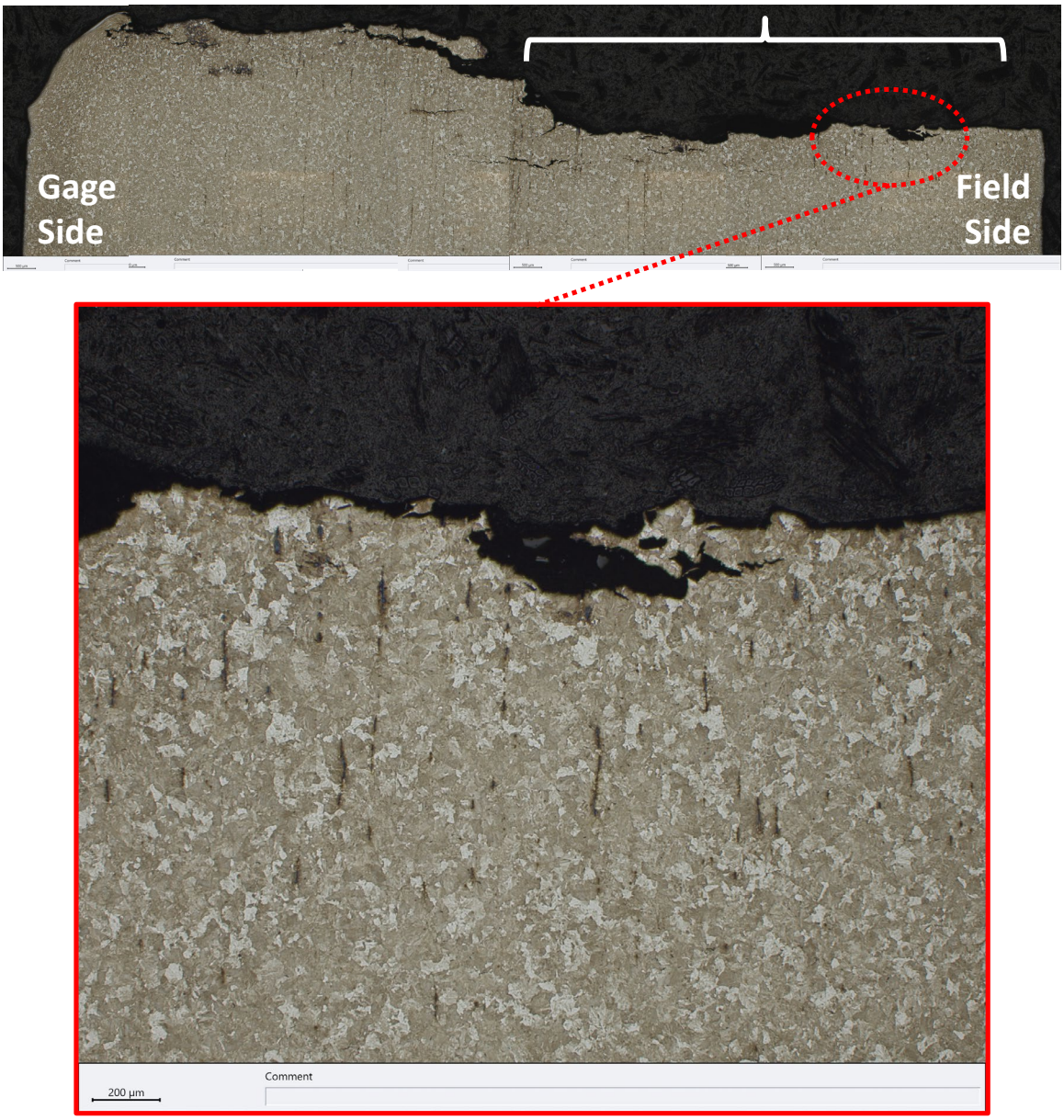

Figure 31: Bright field metallographic images in the web of piece 3W through the anomaly on the fracture surface (white bracket). The microstructure within the anomaly is shown in more detail in the bottom image.
(Etch: 2% Nital)

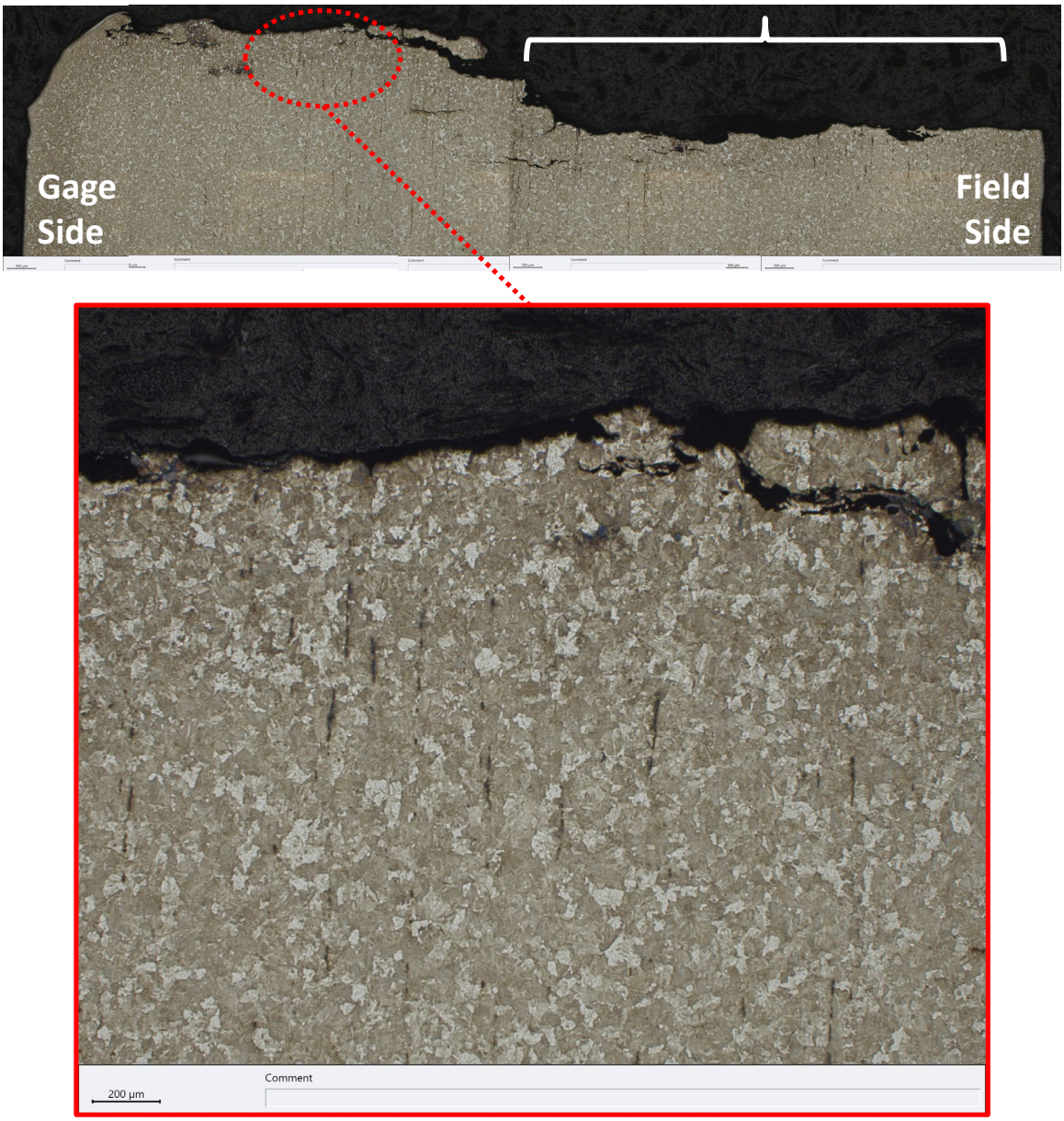

Figure 32: Bright field metallographic images in the web of piece 3W through the anomaly on the fracture surface (white bracket). The microstructure away from the anomaly is shown in more detail in the bottom image.

(Etch: 2% Nital)

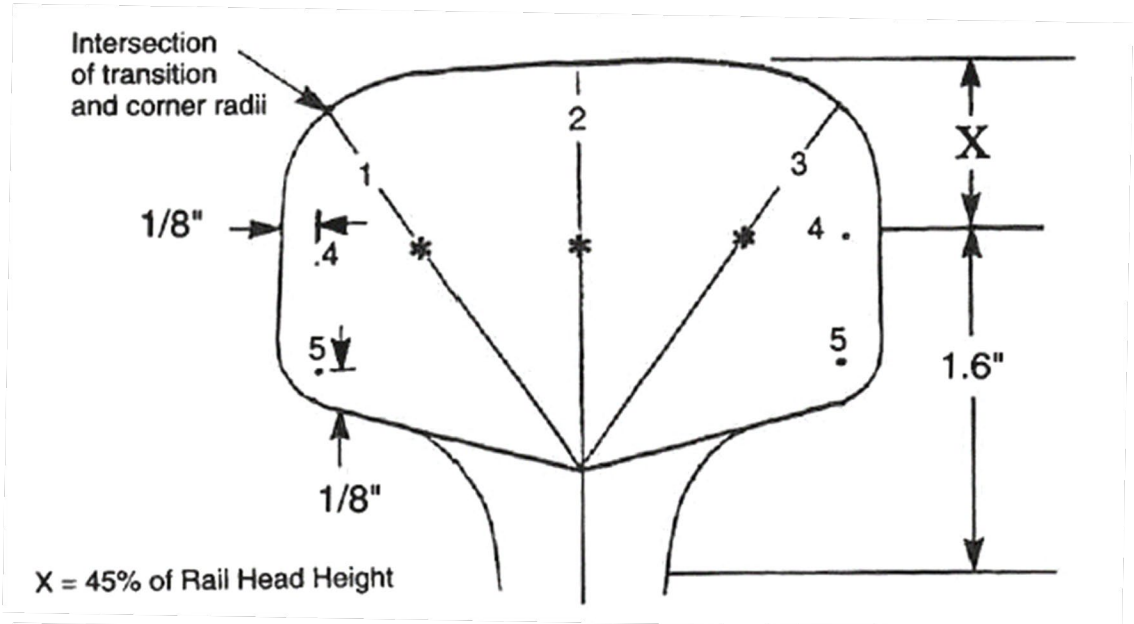

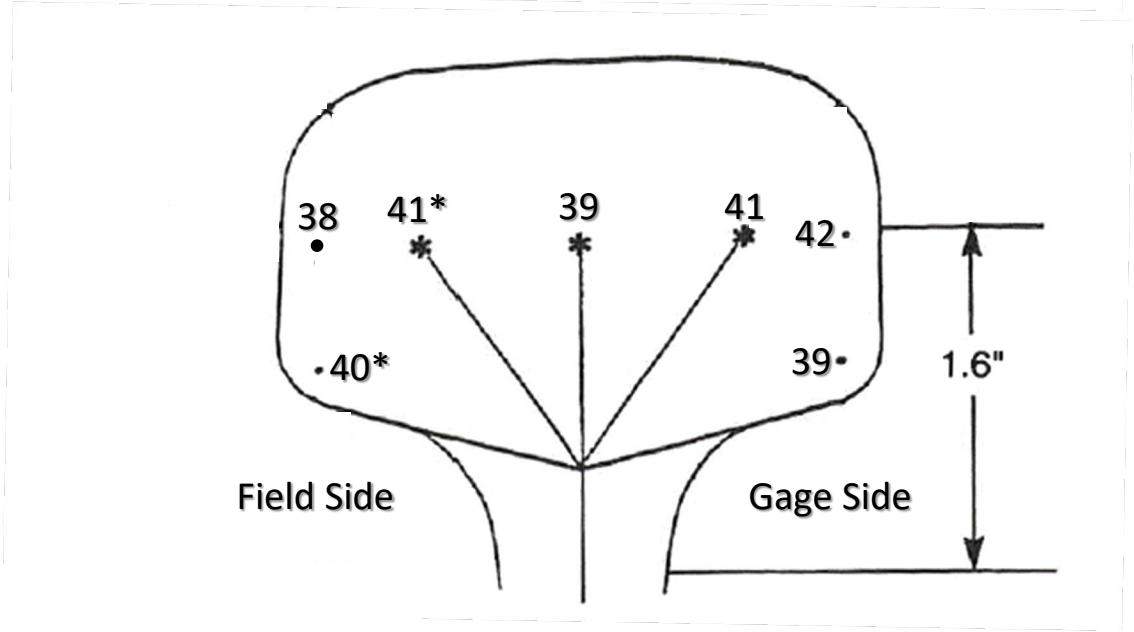

All measurements in HRC
Average hardness: 40 HRC
Standard: 48.0 HRC ± 1.0: 47.2
*These reading were initially 25 and 27 HRC, respectively, but may have been improper tests. Retesting >3 radii away found the results shown

Figure 33: (Top) Diagram showing the seven locations of hardness indents prescribed by AREA for the determination of internal hardness of cross-sectioned rail heads (courtesy, AREA *Manual for Railway Engineering, Chapter 4: Rail*, (1997)).
(Bottom) Diagram showing Rockwell hardness results for the cross-sectioned rail head of piece 3W. All results reported in the HRC scale.

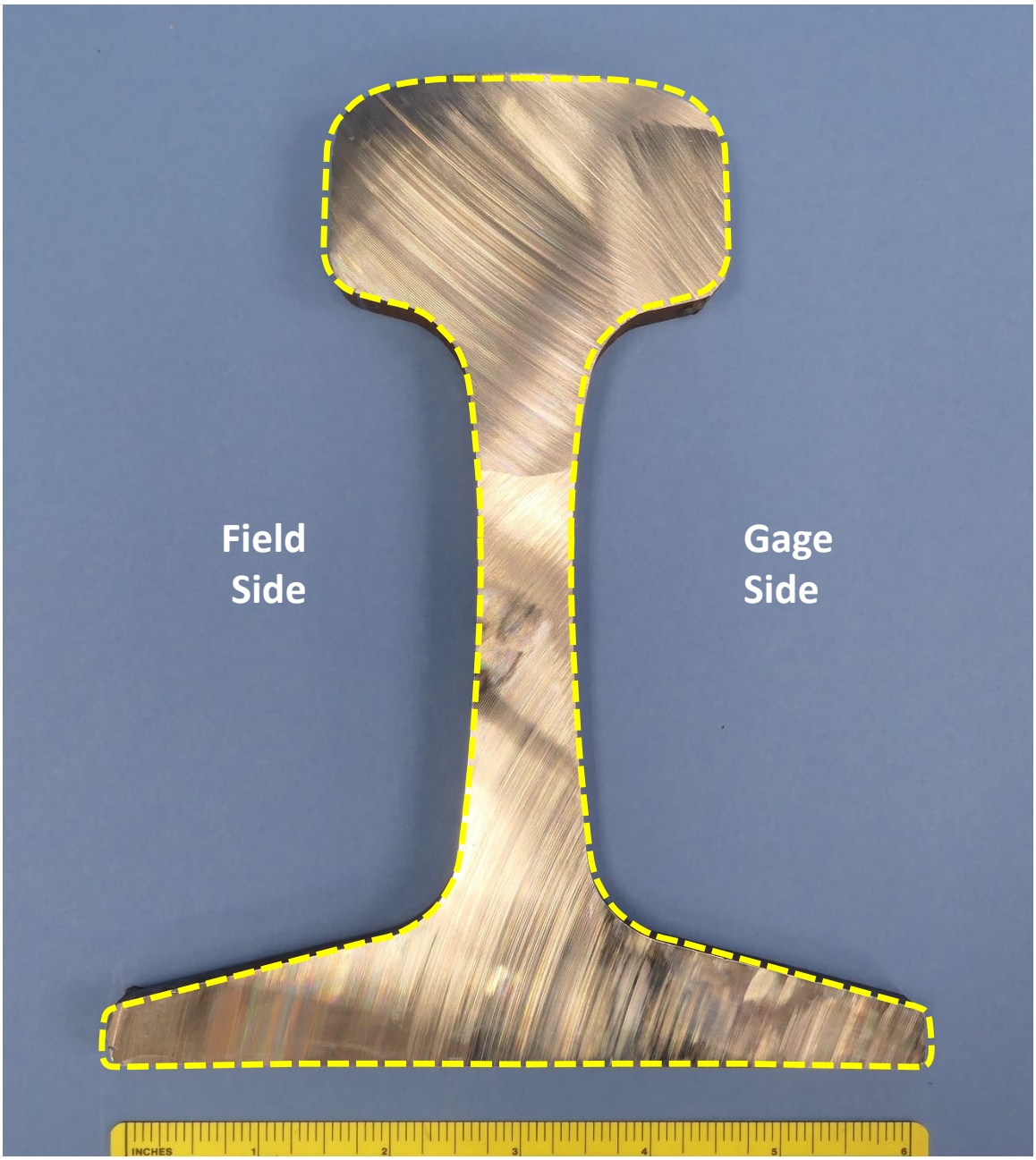

Figure 34: Macro photo of the as-cut surface of transverse rail cross-section slice B from piece 3W with an outline (yellow dashed line) representing the cross-section of a new 136-pound rail overlaid atop.